Tissue-Level Thresholds for Axonal Damage in an Experimental Model of Central Nervous System White Matter Injury

Allison C. Bain

David F. Meaney[1]
e-mail: dmeaney@seas.upenn.edu

Department of Bioengineering,
120 Hayden Hall,
University of Pennsylvania,
Philadelphia, PA 19104-6392

In vivo, tissue-level, mechanical thresholds for axonal injury were determined by comparing morphological injury and electrophysiological impairment to estimated tissue strain in an in vivo model of axonal injury. Axonal injury was produced by dynamically stretching the right optic nerve of an adult male guinea pig to one of seven levels of ocular displacement ($N_{level}=10$; $N_{total}=70$). Morphological injury was detected with neurofilament immunohistochemical staining (NF68, SMI32). Simultaneously, functional injury was determined by the magnitude of the latency shift of the N_{35} peak of the visual evoked potentials (VEPs) recorded before and after stretch. A companion set of in situ experiments ($N_{level}=5$) was used to determine the empirical relationship between the applied ocular displacement and the magnitude of optic nerve stretch. Logistic regression analysis, combined with sensitivity and specificity measures and receiver operating characteristic (ROC) curves were used to predict strain thresholds for axonal injury. From this analysis, we determined three Lagrangian strain-based thresholds for morphological damage to white matter. The liberal threshold, intended to minimize the detection of false positives, was a strain of 0.34, and the conservative threshold strain that minimized the false negative rate was 0.14. The optimal threshold strain criterion that balanced the specificity and sensitivity measures was 0.21. Similar comparisons for electrophysiological impairment produced liberal, conservative, and optimal strain thresholds of 0.28, 0.13, and 0.18, respectively. With these threshold data, it is now possible to predict more accurately the conditions that cause axonal injury in human white matter.
[S0148-0731(00)00906-7]

Keywords: Traumatic Brain Injury, Diffuse Axonal Injury, Injury Tolerance

Introduction

More than two million Americans experience traumatic brain injuries (TBI) every year; nearly 30,000 of these injuries are fatal [1–3]. Despite the reduction in the occurrence and severity of head injury due to the addition of safety features in motor vehicles, as well as improvements in protective helmets, TBI is still the leading cause of death in children and adults under the age of 45, and remains the leading cause of death following motor vehicle accidents [3–5].

The most frequent type of closed head injury, diffuse axonal injury (DAI), accounts for the second largest percentage of deaths due to brain trauma [6–10]. DAI is a type of traumatic brain injury characterized by microscopic damage to axons throughout the white matter of the brain, as well as macroscopic hemorrhages and focal lesions in the corpus callosum and rostral brainstem. The clinical manifestation of these lesions is often immediate, prolonged coma that varies in duration based on the severity and extent of the lesions [7,11,12]. Although treatment paradigms are being developed for DAI, many areas of injury research now focus on developing the tools and techniques needed to prevent DAI.

Central to understanding and evaluating preventive strategies for DAI is determining the tolerance of the brain tissue to mechanical forces. Tissue tolerance data have become important as several finite element models emerge to transfer macroscopic head motions into estimates of the local stress and strain of the intracranial contents [13–19]. When combined, validated finite element models and tissue tolerance data offer a means to identify the hazardous mechanical environments that cause DAI, and provide a tool to aid in the design of countermeasures for reducing the incidence and morbidity of this type of brain injury.

Recent interest in understanding the relationship between tissue stress and strain and the subsequent injury in neural tissue has focused on the tolerance of individual axons and/or axon bundles using in vitro preparations [20–24]. Although demonstrating the clear effect of the mechanical forces on the electrophysiological activity of these tissues, direct extensions of this information to in vivo white matter axons are unclear. In comparison, other studies have employed an integrated modeling approach by comparing spatial mechanical response data of computational and/or physical models to spatial injury patterns from in vivo experiments [15,25]. Although these studies may demonstrate the relationships between local mechanical deformations and injury, they cannot provide exact estimates of the in vivo tissue thresholds because they are hampered by idealizations of the tissue material properties, internal and external geometry, and boundary conditions. In fact, a quantitative strain or stress based in vivo tissue threshold for axonal damage in the central nervous system (CNS) white matter is unknown.

The primary objectives of this investigation are to test the hy-

[1]Corresponding author.

Contributed to the Bioengineering Division for publication in the JOURNAL OF BIOMECHANICAL ENGINEERING. Manuscript received by the Bioengineering Division November 5, 1998; revised manuscript received July 24, 2000. Associate Technical Editor: R. C. Haut.

pothesis that tissue strain is a good predictor of in vivo axonal injury, and to determine the magnitude of tissue strain necessary to cause morphological and functional axonal injury in the guinea pig optic nerve. In this study, we will dynamically displace the optic nerve and examine the morphological and electrophysiological injury exhibited by the nerve. We will then determine a quantitative relationship between applied ocular displacement and the resulting strain in the pre-chiasmatic region of the optic nerve. Finally, these sections will be combined to determine strain based thresholds for in vivo axonal injury.

Methods

Device Description. The device used to stretch the optic nerve delivers a reproducible, measurable amount of uniaxial displacement (0–10 mm) to the globe over a prescribed duration (60 ms, strain rate≈30–60/s) (Fig. 1). Ocular displacement is actuated by a solenoid that is triggered by an electronic circuit, and is measured by a linear variable differential transformer (LVDT) (Trans-Tek Inc., Ellington, CT) connected in parallel with the solenoid. The magnitude of the displacement is controlled by a micromanipulator that adjusts the distance traveled by the solenoid piston. The displacement duration is manually controlled by an external potentiometer. A strain gage force transducer (sensitivity=0.74 mV/Newton) (Entran, Fairfield, NJ) aligned in series with the optic nerve measures the force experienced by the nerve during an experiment. The force and displacement signals are recorded using a computer-based data acquisition system (5 kHz sampling frequency) (Keithley-Metrabyte, Taunton, MA).

Determination of Optic Nerve Strain. Adult, male, albino, Hartley guinea pigs (600–700 g) were euthanized with a lethal dose of sodium pentobarbital (60 mg/kg), and exsanguinated with 0.1 percent heparinized saline. After removing the skullcap and brain, the muscles and connective tissue surrounding the nerve were further discarded to expose both optic nerves. One end of the guinea pig optic nerve is anatomically fixed to the base of the skull via a connective tissue bridge; this connection was left intact. A sling, constructed of sterile surgical material, was placed around the posterior side of the globe so that the optic nerve projected out a slit in the sling. The animal was placed in the optic nerve injury device sterotaxic head holder angled 45 degrees to align the optic nerve in the direction of displacement. The free ends of the sling were connected to the force transducer. The nerve was slightly preloaded (approximately 19.6 mN) to remove any slack. The micromanipulator was adjusted to prescribe the magnitude of ocular displacement. All experiments were performed shortly after sacrifice to minimize post-mortem tissue alterations, and optic nerves were kept hydrated throughout the experiments to better preserve the in vivo state.

Using acrylic paint, small markers were placed at the endpoints of the optic nerve and evenly along its length (four markers total) (Fig. 2(A)). To examine fixation of the endpoint, a fifth point was placed as a reference on the base of the skull. The optic nerve injury device was modified to test the nerve with a ramp (≈30–60/s) and hold (at maximum displacement). A total of seven displacement levels were tested: 2, 3, 4, 5, 6, 7, and 8 mm. These levels encompassed the range of ocular displacements at which nerves were injured in the in vivo experiments. For each displacement level, five separate nerves were photographed while preloaded and at maximum displacement ($N_{total}=35$).

Using the photographs of the preloaded nerve and the nerve at maximum displacement, the gage length of the optic nerve and the displacement of each point with respect to the fixed endpoint were measured with digital calipers (Mitutoyo MTI Corp., Aurora, IL).

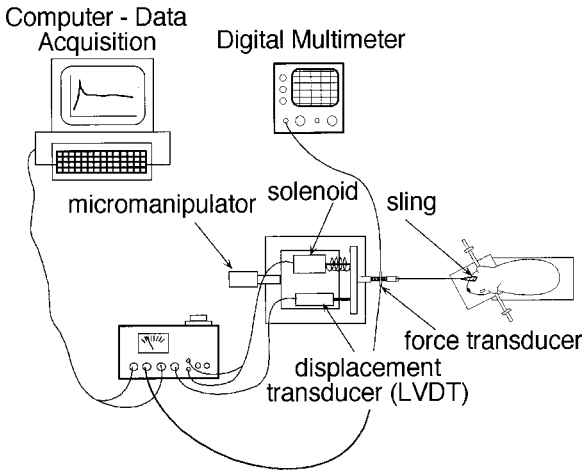

Fig. 1 Schematic of the guinea pig optic nerve stretch model. Elongation is triggered by a solenoid and is measured by a linear variable differential transformer (LVDT). The magnitude of the displacement is controlled by a micromanipulator. The force experienced by the nerve is measured by a strain gauge force transducer aligned in series with the optic nerve. The force transducer is also used in conjunction with a digital multimeter to apply a preload to the optic nerve prior to the experiment.

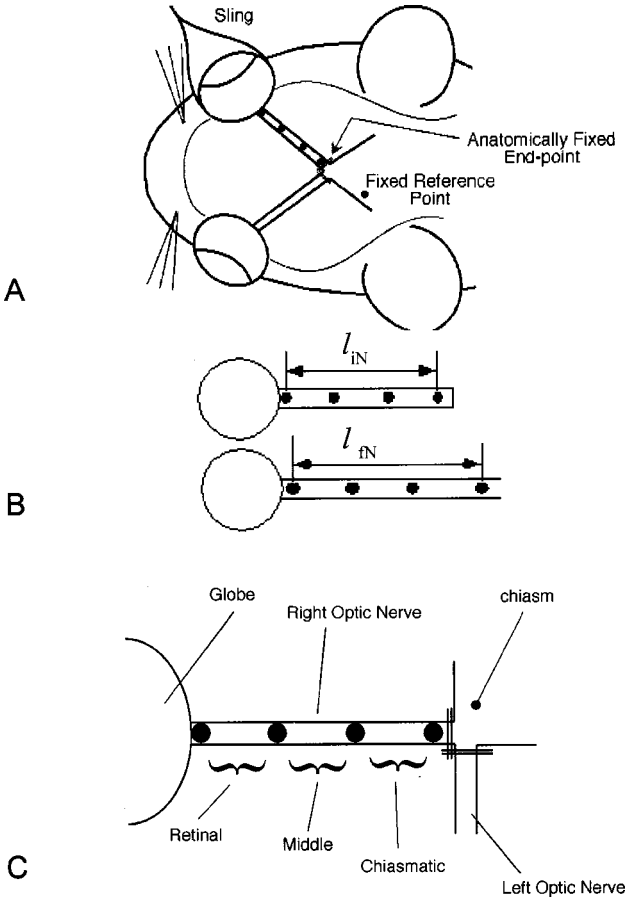

Fig. 2 (A) Schematic of the in situ experiments showing the placement of markers along the length of the nerve, the fixed reference point on the base of the skull, and the end point that is anatomically fixed to the base of the skull. (B) Schematic showing the gage length of the optic nerve (l_{in}), and the measured displacement of the optic nerve after stretch. (C) Schematic of the right optic nerve demonstrating the three areas—retinal, middle, and chiasmatic—used to evaluate the strain uniformity in the nerve.

For each group, the average net nerve displacement was calculated and plotted versus ocular displacement. Linear regression analysis was used to calculate the approximated net nerve displacement for each level of ocular displacement (Kaleidagraph, Synergy Software, Reading, PA). For each in vivo experiment, the approximated length of the nerve at maximum displacement (l_{fN}) and overall the measured nerve gage length (l_{iN}) were used to calculate the Lagrangian strain (E_{11}) experienced by the optic nerve (Fig. 2(B)):

$$E_{11}=\frac{\left(\frac{l_{fN}}{l_{iN}}\right)^2-1}{2} \tag{1}$$

To assess the strain uniformity along the length of the optic nerve, we measured the initial (l_i) and final (l_f) positions, based on the fixed endpoint, of markers in three regions of the optic nerve: the chiasmatic *(c)*, middle *(m)*, and retinal *(r)* regions (Fig. 2(C)). For each region, we calculated the regional stretch ratio (ζ_i) normalized to the overall stretch ratio of the nerve:

$$\zeta_c=\frac{l_{fc}/l_{ic}}{l_{fN}/l_{iN}} \quad \zeta_m=\frac{l_{fm}/l_{im}}{l_{fN}/l_{iN}} \quad \zeta_r=\frac{l_{fr}/l_{ir}}{l_{fN}/l_{iN}} \tag{2}$$

The closer these normalized values were to 1.0, the more uniform the strain field along the length of the pre-chiasmatic nerve section.

For the five nerves tested at each level of ocular displacement, statistically significant differences between the normalized stretch ratios measured in the three regions were detected using a one-way ANOVA and Scheffe's post-hoc analysis (Statistica, Statsoft, Inc., Tulsa, OK). For all tests, significance levels were set at $p<0.05$.

Detecting Morphological Injury. Adult, male, Hartley, albino guinea pigs (600–700 g) were anesthetized with a mixture of ketamine (50 mg/ml) and xylazine (5 mg/ml). The right upper and lower eyelids were injected at the canthi with 2 percent lidocaine and were retracted with suture. Using iris scissors, a 360 deg opening was made in the conjunctiva, and the six extraocular muscle insertions were severed. A sling was placed around the globe and the animal was placed in the injury device in the same manner described previously.

The response of the optic nerve to dynamic tensile stretch was examined for six ocular displacement groups: 3, 4, 5, 6, 7, and 8 mm stretch. These groups were chosen based on the results of a set of preliminary studies that were conducted to define the levels of ocular displacement necessary to produce a range of injury responses, from no electrophysiological impairment or axonal damage to immediate changes in the visual evoked potential and extensive signs of axonal damage in the nerve at three days post-stretch. Ten animals were tested in each displacement group, and an additional group of ten animals served as surgical sham controls. Following injury, the sling was cut free from the force transducer, the animal was removed from the head holder, and the sling was removed from the globe. The animal was monitored until it was completely ambulatory and was then returned to the animal facility. All surgical techniques were approved by the University of Pennsylvania's Institutional Animal Care and Use Committee (IACUC).

Three days post-injury, the animal was euthanized with a lethal dose of sodium pentobarbital (60 mg/kg), exsanguinated with 0.1 percent heparinized saline, and perfused with 10 percent neutral buffered formalin followed by 10 percent sucrose saline. Both left and right optic nerves were removed and post-fixed in 10 percent neutral buffered formalin for 24 h. The optic nerves were then dissected free of extraocular muscles, glandular tissue, and dural sheaths and stored in 30 percent sucrose. The nerves were cut on a freezing microtome into two sets of longitudinal sections 16 μm thick, and stored in phosphate buffered saline (PBS) for no longer than 24 h. We used a common technique, detection of neurofilament proteins in the axonal cytoskeleton, to identify traumatic axonal damage [26–32]. One set of sections from each nerve was stained using the monoclonal antibody NF 68 (Sigma Chemical Company, St. Louis, MO), which stains light weight neurofilament proteins (68 kD). The second set was stained using SMI 32, which stains non-phosphorylated medium and heavy weight neurofilament proteins. Both sets of sections were mounted on slides and cover-slipped, and examined for injury with light microscopy using a 40× objective. Each nerve was analyzed and given an injury score of 1 or 0 based on the presence (1) or absence (0) of axonal swellings or retraction balls in any section of the nerve.

Detecting Functional Impairment. The functional impairment of the optic nerve was assessed by measuring changes in electrical potentials generated by the retinal ganglion cells and transmitted to the visual cortex via the optic nerve, termed visual evoked potentials (VEPs). A VEP trace (~200 ms duration) is a characteristic series of positive and negative voltage peaks that occur at defined time intervals. Functional impairment of the optic nerve is indicated when these characteristic peaks occur later than normal [33–36]. Nearly all of the axons in the albino guinea pig optic nerve (~97 percent) cross at the optic chiasm and traverse to the contralateral visual cortex [37–40]. Hence, VEPs measured at one side of the occipital cortex represent the signals conducted by the contralateral optic nerve. This was verified in a preliminary set of experiments in which a flat-line VEP was measured from the occipital cortex after the contralateral nerve was transected.

Prior to surgery, two sterile needle electrodes were inserted under the scalp over the left and right visual cortex, 5 mm lateral to the midline and 2 mm anterior to the lamboidal point. A third reference electrode was clipped to the left ear, and a ground electrode was attached to the right foot. The animal was placed in a grounded Faraday cage and was dark-adapted for four min prior to each set of VEP measurements [34,41–44]. After dark-adaptation, a photostimulator presented unpatterned flashes from a lamp placed 20 cm from the right eye at a rate of 1.0 Hz (Grass Instruments, Astro-Med, Inc., West Warwick, RI). The flash was directed at the right eye via a black cone placed over the lamp that prevented the left eye from being stimulated. Each flash elicited the recording of the potential generated at the left visual cortex with respect to the reference electrode. Each signal was pre-amplified (1000×) and measured (2 kHz sampling rate) for 500 ms post-flash.

Three control VEPs were measured prior to the surgical preparations and stretch. After stretch, the animal was quickly removed from the stretch apparatus, placed in the Faraday cage, and dark adapted. The first VEP recording after stretch occurred at 8 min post-injury. Subsequent post-injury VEPs were recorded every 5 min thereafter, ending at 48 min, and at sacrifice (72 h). For each recording time point, a set of 64 VEPs (one VEP per flash) was recorded by a computer-based data acquisition system (2 kHz sampling rate). Each set of 64 VEPs was averaged to produce one VEP recording per time point. VEPs were measured in 30 of the 60 animals injured at six different levels of ocular displacement and in a set of sham animals ($N_{\text{level}}=5$, $N_{\text{total}}=35$).

All signals were digitally filtered with a Chebyshev 1–100 Hz bandpass filter (Matlab, Mathworks, Inc., Natick, MA). For each signal, the latency of the N_{35} peak was recorded. The latency shift of the N_{35} peak was calculated as the increase in latency from the pre-stretch level. The mean and standard deviation of the latency of the N_{35} peak in VEPs measured from sham animals were calculated and used to define presence or absence of functional injury. Similar to the morphological injury analysis, we assigned a functional injury status to each nerve at every time point based on the magnitude of the measured latency shift. All latency shift recordings that fell outside two standard deviations of the average sham recording were labeled as injured (1); all other recordings were considered uninjured (0).

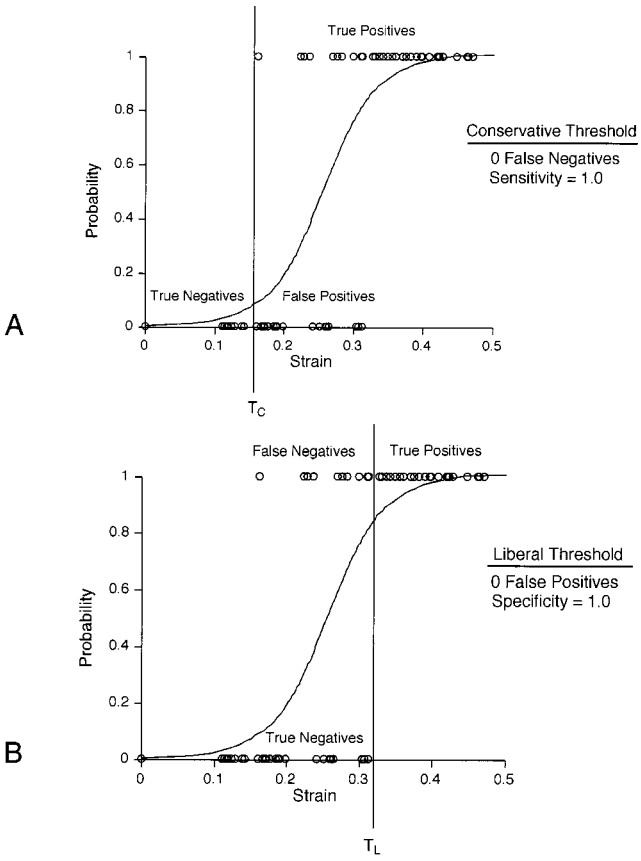

Fig. 3 Representation of the conservative (A) and liberal (B) thresholds calculated for morphological and functional injury. Below the conservative threshold, no nerves will be injured; therefore, there are no false negatives and the threshold achieves a sensitivity of 1.0. Above the liberal threshold, all nerves will exhibit injury and therefore there are no false positives, yielding a specificity of 1.0.

Determining Injury Thresholds. For each in vivo experiment, optic nerve strain was estimated using the predicted net displacement of the in situ optic nerve, and the gage length of the pre-chiasmatic nerve measured at sacrifice. Morphological injury status and functional injury status at each recording time point were plotted versus this estimated optic nerve strain. Logistic regression analysis was performed to predict strain thresholds for morphological injury and for functional injury at the different time points (SYSTAT LOGIT Plus-in Module, SPSS, Inc., Chicago, IL). The logistic regression fit was considered significant for chi-squared values with $p<0.05$. Also, McFadden's rho-squared value, similar to the correlation coefficient in linear regression, was used to evaluate the ability to represent the data with a logistic regression.

Sensitivity and Specificity Analysis of Thresholds. For each logistic regression analysis, we calculated the sensitivity and specificity of the predicted strain values at 15 different probability levels [45]. For each probability level, we recorded the number of true positives (TP), false positives (FP), true negatives (TN), and false negatives (FN) based on whether or not the optic nerve strain recorded for that experiment was above or below the threshold value and whether or not the animal exhibited injury. The sensitivity and specificity of the particular threshold were then calculated using:

$$\text{Sensitivity}=\frac{TP}{TP+FN} \tag{3}$$

$$\text{Specificity}=\frac{TN}{FP+TN} \tag{4}$$

In addition, a receiver operating characteristic (ROC) curve was constructed by plotting sensitivity versus 1-specificity for the different probability values [45–51]. The area under each ROC curve (AUC) was calculated and reported as a fraction of the maximum possible area. The AUC is a normalized measure of the ability of optic nerve strain to discriminate between injured and uninjured nerves. A measure that predicts outcome 100 percent of the time has an AUC of 1.0; a measure that lacks discriminatory power, or predicts outcome no better than random guessing, has an AUC of 0.50 [52–60].

The ROC curve was also used, in combination with a plot of the sum of the sensitivity and specificity versus the various probability values, to determine specific cutoff points to be used as thresholds for morphological and functional axonal injury [46,49,51,52,55]. Specifically, the ROC curves were used to define three potentially useful thresholds. First, we defined a ''liberal'' threshold (T_L) by the point on the ROC curve where the sensitivity attained its highest value at a specificity of 1.0 (Fig. 3(A)). This threshold represents the point above which all nerves exhibit injury. Second, we defined a ''conservative'' threshold (T_C) by a point on the ROC curve where the specificity reached its highest value at a sensitivity equal to 1.0 (Fig. 3(B)). Below this threshold, no nerves exhibit injury. Lastly, we define an ''optimal,'' or best, threshold (T_B), defined by the probability that maximizes the sum of the specificity and sensitivity [56].

Results

In situ Displacement-Stretch Relationship. For each in situ experiment, we calculated the displacement of the nerve based on the change in distance between the nerve's marked endpoints. The anatomically fixed endpoint remained stationary for all experiments except those in the 8 mm stretch group. The slight movement of this fixed endpoint was accounted for in the nerve displacement measurements for these experiments. For ocular displacements between 2 and 8 mm, the measured nerve displacements were between 0.5 and 3.0 mm. The nerve displacements increased with increasing levels of ocular displacement, but were noticeably lower than the prescribed ocular displacements (Fig. 4). We also observed that the precision of nerve displacements decreased with increasing ocular displacement. However, the data was approximated by a straight line with a very high correlation coefficient ($R=0.99$). This regression produced approximate nerve displacements that fell within one standard deviation of the measured displacements for all but two levels of ocular displacement.

The mean gage length ($\pm$standard deviation) measured for all nerves injured in the in vivo experiments was 8.40 ± 0.59 mm. When combined with the approximated nerve displacements, these gage lengths corresponded to nerve strains (E_{11}) between 0.10 and 0.50 for ocular displacements between 3–8 mm.

Strain Uniformity. Although normalized stretch ratios measured in the three different nerve regions varied slightly within a nerve, this variation was not consistent among different nerves. ANOVA analysis found a statistically significant difference in normalized stretch ratios in only one (6 mm) of the seven ocular displacement groups. In the 6 mm group, normalized stretch ratios measured in the chiasmatic region (average normalized stretch ratio=0.98) were smaller than those measured in the middle (average normalized stretch ratio=1.03) and retinal region (average normalized stretch ratio=1.004) ($p=0.0008$). Despite this significant difference, the average deviation in regional strain at this level of stretch was only 0.025 m/m, approximately 3 percent of the average stretch value for this group.

Thresholds for Morphological Injury. Of the 70 in vivo experiments, axonal pathology was detected in 33 of 70 nerves.

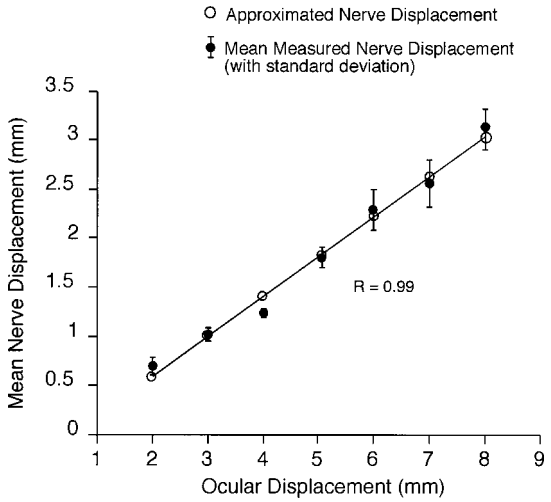

Fig. 4 Results of the in situ displacement-stretch experiments. The mean measured nerve displacements (dark circles) were plotted versus the applied ocular displacement. Linear regression was used to develop a relationship ($R=0.99$) between the applied displacement and resulting net displacement of the optic nerve; predicted nerve displacements fell within one standard deviation of measured for all but one level of ocular displacement.

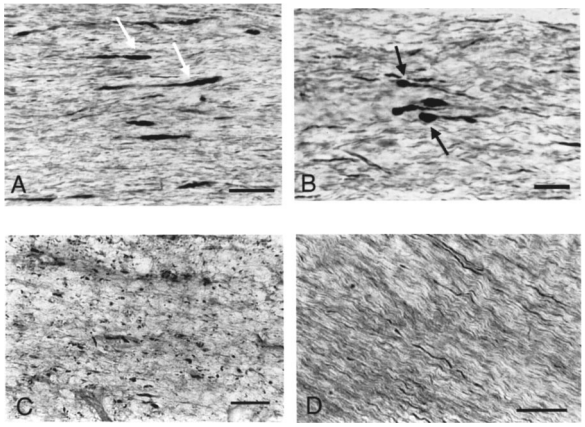

Fig. 5 (A,B) Longitudinal optic nerve sections injured at 7 mm and stained with NF68, a marker for axonal pathology. Injured nerves exhibited clusters of retraction bulbs (black arrows) and axonal swellings (white arrows) near the retina and 1–2 mm from the chiasm. (C) Longitudinal section injured at 8 mm and stained with SMI32. At higher injury levels, degeneration fragments were observed. (D) Longitudinal section of an uninjured nerve stained with SMI32. Bar: (A) 40 μm, (B) 20 μm, (C,D) 40 μm.

Nerves injured at levels below 4 mm did not exhibit any injury, whereas all nerves subjected to stretch levels above 6 mm demonstrated injury (Fig. 5). In one animal injured at 4 mm, a low frequency of both axonal swellings (<5 per nerve section) and retraction bulbs (<5 per nerve section) was observed near the retina. As the stretch level was increased, the density of axonal abnormalities at the retina increased, and axonal pathology started to appear in clusters 1–2 mm from the chiasm. At the highest stretch levels, isolated retraction bulbs and axonal pathology were also frequently found along the length of injured nerves.

Logistic Regression Analysis. Logistic regression of the in vivo morphological injury data versus the estimated nerve strain demonstrated high significance in the estimation of the logit parameters (Likelihood Ratio Test, chi-squared, $p<0.0001$). Also, McFadden's rho-squared value was considered highly significant (0.60) [61,62].

Threshold Analysis. The specificity of the predicted threshold strain, calculated for varying probability values of the morphological injury logistic regression, increased with increasing probability level, whereas the sensitivity decreased. The area under the ROC curve was 0.95, suggesting that optic nerve strain is a very good predictor of morphological injury. The conservative threshold was defined by the 5 percent probability value on the ROC curve, and corresponded to a threshold strain of 0.14 (95 percent confidence limits (CL)=0.04, 0.18) (Fig. 6). The 90 percent probability value, or a threshold strain of 0.34 (CL=0.30, 0.42), defined the liberal threshold for morphological injury. By evaluating the sum of the sensitivity and specificity, we found that the best overall threshold for predicting morphological injury was defined by the 25 percent probability value or a strain value of 0.21 (CL =0.16, 0.24).

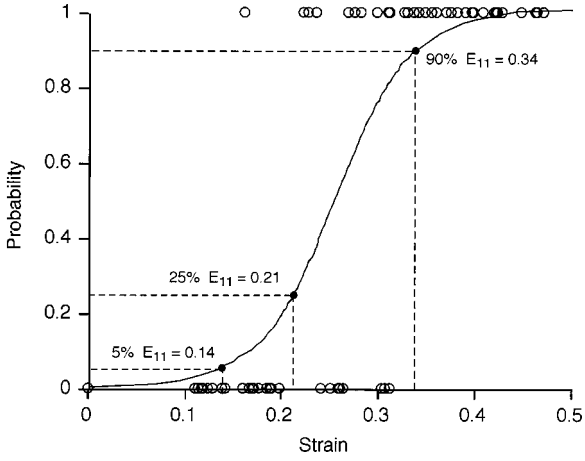

Fig. 6 Logit analysis of morphological injury data. Nerves were labeled either injured (probability=1) or uninjured (probability=0) based on the presence or absence of morphological injury. Logit parameters were estimated with very high significance (likelihood ratio test, chi-squared, $p<0.0001$). The results of this analysis were used to define a conservative threshold ($E_{11}=0.14$, 95 percent confidence limits (CL)=0.04, 0.18), a liberal threshold ($E_{11}=0.34$, CL=0.16, 0.24), and the best, or optimal threshold ($E_{11}=0.21$, CL=0.30, 0.42) for morphological injury.

Thresholds for Electrophysiological Impairment. Pre-injury VEPs were consistent among animals and between pre-injury trials, and were very similar to those recorded by other investigators [41–44,63]. The mean latency (±standard deviation) of the N_{35} peak in pre-injury recordings was 34.8 ms (±1.1 ms). At all levels of ocular displacement, functional impairment of the optic nerve was noted at the earliest time point after injury (8 min), as indicated by a latency shift of the N_{35} peak. Nerves injured at higher levels of ocular displacement generally showed greater degrees of N_{35} latency shift. In most cases, N_{35} latency gradually decreased after injury, and returned to pre-injury levels by 72 h.

Logistic Regression Analysis. Logistic regression analysis of electrophysiological impairment data versus estimated tissue strain demonstrated high significance in estimating the model parameters (Likelihood Ratio Test, chi-squared, $p<0.001$) at all time points except 72 h. Also, McFadden's rho-squared values were very high for all time points up to 43 min (0.45–0.79). It was clear from this analysis that values predicted at 48 min and 72 h lacked the statistical significance to predict thresholds for injury confidently; therefore, we only evaluated threshold values obtained by measurements up to 43 min post-injury.

Threshold Analysis. For the eight time points being considered,

the sensitivity and specificity for varying probabilities were used to construct eight separate ROC curves. The area under the ROC curve was greater than 0.94 at these time points, with the highest AUC value occurring at 23 min. This indicated that optic nerve strain is a very good indicator of functional impairment measured by latency shifts from VEPs recorded up to 43 min after injury. Conservative threshold values for electrophysiological impairment corresponded to strains between 0.09 and 0.18, with an average conservative threshold strain ($\pm$standard deviation) of 0.13 ($\pm$0.06). In comparison, liberal thresholds for impairment ranged from 0.18 to 0.47, with an average liberal threshold strain of 0.28 ($\pm$0.13). Finally, the optimal threshold ranged from 0.17 to 0.19 across all time points, with an average strain of 0.181 ($\pm$0.02). The average of the thresholds for impairment across all time points were significantly different (ANOVA, $p<0.05$).

Discussion

In this investigation, we demonstrated the correlation between the strains experienced in the guinea pig optic nerve with morphological and functional injury. From these analyses, we also showed that there are unique values of strain, above which optic nerves will exhibit immunohistochemical evidence of injury and electrophysiological impairment. Subsequently, we determined three strain-based thresholds for morphological damage in white matter. The first (liberal) threshold strain of 0.34 produced a specificity of 1.00, and refers to the strain above which all nerves are predicted to exhibit injury. Conversely, the second (conservative) threshold prediction of 0.14 produced a sensitivity of 1.00 and defines the strain below which no nerves will show injury. The final (optimal) threshold criteria of 0.21 optimized both the specificity and sensitivity.

A similar analysis of electrophysiological impairment produced different threshold strains for each of the time points because we observed a gradual recovery of the peak latencies as time progressed, with many latencies returning to normal, pre-injury levels by sacrifice (72 h). This might indicate that individual axons exhibited transient functional impairment but ultimately recovered full function, or that the uninjured axons compensated for the injured axons and were able to reestablish normal function. The temporal recovery of the VEP waveform precluded determining a unique threshold for electrophysiological impairment. The thresholds strains predicted for functional impairment ranged from 0.09 to 0.47, with average liberal, conservative, and optimal strain thresholds of 0.28, 0.13, and 0.18, respectively. The threshold strains predicted for impairment at 23 and 28 min post-injury were most similar to those predicted for morphological injury. Also, the correlation between electrophysiological impairment and optic nerve strain, as indicated by McFadden's rho-squared value, was highest at these same time points. Although this suggested that VEPs recorded 23–28 min post-injury may provide the most reliable and useful information for predicting the degree of morphological injury, the specific relationship between morphology and function is still unclear.

In addition to developing thresholds for axonal injury, this investigation has expanded on this information by critically analyzing the chosen thresholds using measures of sensitivity, specificity, and ROC curves. These techniques have been used extensively in clinical research to assess the efficacy of different pharmocological drugs, treatments paradigms, and to evaluate the performance of diagnostic tests [46,48–52,54–60,64–67]. Although these tools have also been used to some extent to determine the effectiveness of different injury severity scoring systems, they have not been employed explicitly to evaluate how well proposed thresholds or tolerances for injury perform in practice [47,67].

In the current study, we used the ROC curves to identify three individual strain-based thresholds that take these considerations into account. Although these thresholds have different strengths and limitations, each has the potential to play a unique and valuable role in the study of head injury. For example, the liberal threshold may be used in combination with a finite element simulation of an experimental brain injury model to determine the loading conditions necessary to consistently produce injury in the experimental model. Conversely, the conservative threshold may be used with a finite element model to define standards for prevention of human head injury—a situation where researchers may opt to overestimate the likelihood of injury. The optimal threshold balances the advantages and disadvantages of the liberal and conservative thresholds and may be more appropriate as a general prognostic tool that provides the best overall predictive value. Although the development of a single threshold for axonal injury seems appropriate, the selection of a threshold to use in practice ultimately depends on the specific application and the penalties associated with false positive or false negative predictions.

This investigation represents the first study that determines thresholds based on experimental measurement of strain from central nervous system tissue. In the past, estimates for the tolerance of white matter tissue were derived from a combination of an experimental model with a physical or computational model to estimate the strains experienced by the tissue. For example, Mendis [15] matched oriented strain values determined from a finite element model of the primate brain to experimental injury, and found moderate DAI to occur at strains of 28 percent. Also, in a similar analysis, strains observed in a physical model of inertial injury were compared to injury in a primate brain to arrive at shear strain thresholds for moderate to severe DAI of 9.4 percent [25]. In both investigations, the limitations of the physical and computational methods were recognized. Assumptions about the boundary conditions and the brain material properties and geometry affect the measured or predicted intracranial deformations. Validating the model's response with experimentally measured variables increases the reliability of strain approximations; however, it is very difficult and frequently impossible to make experimental measurements in many models of axonal injury.

By using the guinea pig optic nerve model, we were able to alleviate the concerns raised in previous investigations of white matter tolerances. We determined the strain experienced by the optic nerve from in situ experiments that were very similar to the in vivo condition. In these experiments we observed that the measured optic nerve displacement is noticeably lower than the applied ocular displacement. This result was caused by several factors. Most importantly, we expected that a percentage of the applied ocular displacement would be transferred to the globe. Although we did not attempt to quantify this percentage, photographs of the in situ experiments suggested that the globe did experience some deformation. Examination of the in situ photographs also revealed that the sling did not constitute a perfect couple between the device and the optic nerve. In preliminary in vivo experiments, we recognized that when the sling was secured tightly around the globe, the blood supply to the retina was hindered. By not securing the sling tightly, we introduced some slip into the system that was apparent in the in situ photographs. Both of these factors contributed to the observed decrease in nerve displacement when compared to the applied ocular displacement. Therefore, identifying the correct transfer function between the ocular displacement and the nerve displacement was a critical step in relating the observed injury to the tissue level strain.

We also used the in situ experiments to show that the strain field in the optic nerve is primarily uniform within the range of displacements utilized in the in vivo experiments. Unlike many biological tissues, which often exhibit nonuniform strain patterns, the optic nerve has a very regular geometry with a cross-sectional area and microstructure that are relatively constant along the length of the nerve [68]. These characteristics are most likely responsible for the uniform strain patterns we observed in the in situ experiments. The uniformity obviated the need to compare

specific strain patterns to regional variation in injury within the tissue; thus, the location of detectable injury was unimportant toward the determination of an injury threshold.

A limitation of this study is the use of single outcome measures for morphological and functional damage to the optic nerve. To focus the study, we chose the most frequently used markers of damage to the white matter—accumulation of neurofilament proteins and changes in the visual evoked potential—to develop the thresholds. Although other immunocytochemical techniques are used for detecting axonal pathology, the change in neurofilament staining allows the direct transfer of the thresholds to the next stage: predicting the distribution of injury in experimental models of brain injury (see [69]) as well as in cases of human brain injury. Also, while other behaviorally based measures were available to assess changes in the visual system after stretch, the dissection of the extraocular muscles in our current surgical preparation precluded the use of these measures in our study. Therefore, the strain thresholds predicted in this investigation may apply only to morphological axonal injury detected by NF68 and SMI-32 and electrophysiological impairment indicated by changes in peak latency in VEPs.

The accuracy of the predicted strain thresholds depends on limitations of the in situ experiments. The in situ behavior of the optic nerve is only an estimate of the actual in vivo behavior, it is currently impossible to know explicitly the strain that the optic nerve experienced during an in vivo experiment. However, every effort was made to replicate the in vivo environment. The experiments were conducted shortly after sacrifice to minimize post mortem tissue alterations, and the optic nerves were kept hydrated throughout the experiments. Also, we reproduced the exact biomechanical parameters (head orientation, nerve preload) used in the in vivo experiments. Thus, while still an estimate, we believe that our results are an accurate portrayal of the in vivo dynamics of the optic nerve during stretch.

Finally, it is important to recognize that the tissue-level thresholds for injury presented herein are based on the guinea pig optic nerve, and may or may not be directly applicable to human axonal injury. Evidence suggests that the mechanical behavior of CNS tissue does not vary significantly from species to species, so that strain-based injury criteria may be very similar between species [70]. However, while tissue-level thresholds for white matter may be independent of the particular species, they may also be strongly dependent on the microstructural arrangement of the axons within the tissue. Axons in the guinea pig optic nerve are undulated [71]. This undulation could potentially affect the strain necessary to produce injury, depending on the kinematics of the individual axons during stretch. We are characterizing currently the distribution of axonal undulation in the guinea pig optic nerve at different levels of stretch. This examination of the microstructural kinematics in the guinea pig optic nerve would assist in defining strain-based injury criteria for individual axons. Axon-level thresholds are independent of both global and local geometries, and therefore, could be more universally applicable to the study of human head injury.

Acknowledgments

The authors would like to acknowledge the support of the Centers for Disease Control (CCR312712), the N.I.H. (NS35712), and the Whitaker Foundation.

References

[1] Sosin, D., Sniezek, J., and Waxweiler, R., 1995, ''Trends in Death Associated With Traumatic Brain Injury, 1979 Through 1992: Success and Failure,'' J. Am. Med. Assoc., **273**, pp. 1778–1780.

[2] Sosin, D., Sacks, J., and Smith, S., 1989, ''Head Injury—Associated Deaths in the United States From 1979–1986,'' J. Am. Med. Assoc., **262**, pp. 2251–2255.

[3] Pope, A. M., and Tailor, A. R., 1991, *Disability in America: Toward a National Agenda for Prevention*, National Academy Press, Washington, DC.

[4] Kraus, J. F., Black, M. A., Hessol, N., Ley, P., Rokaw, W., Sullivan, C., Bowers, S., Knowlton, S., and Marshall, L., 1984, ''The Incidence of Acute Brain Injury and Serious Impairment in a Defined Population,'' Am. J. Epidemiol., **119**, pp. 186–201.

[5] Sauaia, A., Moore, F. A., Moore, E. E., Moser, K. S., Brennan, R. A., and Pons, P. T., 1995, ''Epidemiology of Trauma Deaths: A Reassessment,'' J. Trauma: Inj., Infect., Crit. Care, **38**, pp. 185–193.

[6] Adams, J. H., Doyle, D., Ford, I., Gennarelli, T. A., and Graham, D. I., 1989, ''Diffuse Axonal Injury in Head Injury: Definition, Diagnosis and Grading,'' Histopathology, **15**, pp. 49–59.

[7] Gennarelli, T. A., Thibault, L. E., Adams, J. H., Graham, D. I., Thompson, C. J., and Marcinin, R. P., 1982, ''Diffuse Axonal Injury and Traumatic Coma in the Primate,'' Ann. Neurol., **12**, pp. 564–574.

[8] Gennarelli, T. A., Segawa, H., Wald, U., Czernicki, Z., Marsh, K., and Thompson, C., 1982, ''Physiological Response to Angular Acceleration of the Head,'' in: *Head Injury: Basic and Clinical Aspects*, R. Grossman and P. Gildenberg, eds., Raven Press, New York, pp. 129–140.

[9] Adams, J. H., Gennarelli, T. A., Graham, D. I., Scott, G., and Thibault, L. E., 1983, ''Diffuse Axonal Head Injury in Non-Missile Head Injury,'' in: *Advances in Neurotraumatology*, R. Villiani, ed., Excerpta Medica, Amsterdam, pp. 53–58.

[10] Gentleman, S. M., Roberts, G. W., Gennarelli, T. A., Maxwell, W. L., Adams, J. H., Kerr, S., and Graham, D. I., 1995, ''Axonal Injury: A Universal Consequence of Fatal Closed Head Injury?'' Acta Neuropathol. (Berl), **89**, pp. 537–543.

[11] Gennarelli, T. A., 1983, ''Head Injury in Man and Experimental Animals: Clinical Aspects,'' Acta Neurochir., **32**, pp. 1–13.

[12] Adams, J. H., Graham, D. I., and Gennarelli, T. A., 1981, ''Acceleration Induced Head Injury in the Monkey. II. Neuropathology,'' Acta Neuropathol. Suppl. (Berl), **7**, pp. 26–28.

[13] Zhou, C., Khalil, T. B., and King, A. I., 1994, ''Shear Stress Distribution in the Porcine Brain Due to Rotational Impact,'' in: *Proc. 38th Stapp Car Crash Conference*, SAE, Ft. Lauderdale, FL.

[14] Ruan, J. S., Khalil, T., and King, A. I., 1991, ''Human Head Dynamic Response to Side Impact by Finite Element Modeling,'' ASME J. Biomech. Eng., **113**, pp. 276–283.

[15] Mendis, K., 1992, ''Finite Element Modeling of the Brain to Establish Diffuse Axonal Injury Criteria,'' thesis, Ohio State University.

[16] Chu, C. S., Lin, M. S., Huang, H. M., and Lee, M. C., 1993, ''Finite Element Analysis of Cerebral Contusion,'' J. Biomech., **27**, pp. 187–194.

[17] Bandak, F. A., and Eppinger, R. H., 1994, ''A Three-Dimensional Finite Element Analysis of the Human Brain Under Combined Rotational and Translational Accelerations,'' in: *Proc. 38th Stapp Car Crash Conference*, SAE, Fort Lauderdale, FL.

[18] Ueno, K., Melvin, J. W., Li, L., and Lighthall, J. W., 1995, ''Development of Tissue Level Brain Injury Criteria by Finite Element Analysis,'' J. Neurotrauma, **12**, pp. 695–706.

[19] Shreiber, D. I. and Meaney, D. F., 1998, ''Finite Element Analysis of Traumatic Brain Injury in the Rat,'' ASME J. Biomech. Eng., submitted.

[20] Gray, J. A. B., and Ritchie, J. M., 1954, ''Effects of Stretch on Single Myelinated Nerve Fibers,'' J. Physiol. (Lond), **124**, pp. 84–99.

[21] Galbraith, J. A., Thibault, L. E., and Matteson, D. R., 1993, ''Mechanical and Electrical Responses of the Squid Giant Axon to Simple Elongation,'' ASME J. Biomech. Eng., **115**, pp. 13–22.

[22] Haftek, J., 1970, ''Stretch Injury of Peripheral Nerve,'' J. Bone Jt. Surg., Br. Vol., **52B**, pp. 354–365.

[23] Koike, H., 1987, ''The Extensibility of Aplysia Nerve and the Determination of True Axon Length,'' J. Physiol. (Lond), **390**, pp. 469–487.

[24] Saatman, K. E., 1993, ''An Isolated Single Myelinated Nerve Fiber Model for the Biomechanics of Axonal Injury,'' thesis, University of Pennsylvania.

[25] Margulies, S. S., and Thibault, L. E., 1992, ''A Proposed Tolerance Criterion for Diffuse Axonal Injury in Man,'' J. Biomech., **25**, pp. 917–923.

[26] Yaghmai, A., and Povlishock, J. T., 1992, ''Traumatically Induced Reactive Change as Visualized Through the Use of Monoclonal Antibodies Targeted to Neurofilament Subunits,'' J. Neuropathol. Exp. Neurol., **51**, pp. 158–176.

[27] Sternberger, L. A., and Sternberger, N. H., 1983, ''Monoclonal Antibodies Distinguish Phosphorylated and Nonphosphorylated Forms of Neurofilaments in situ,'' Proc. Natl. Acad. Sci. U.S.A., **80**, pp. 6126–6130.

[28] Ross, D. T., Meaney, D. F., Sabol, M. K., Smith, D. H., and Gennarelli, T. A., 1994, ''Distribution of Forebrain Diffuse Axonal Injury Following Inertial Closed Head Injury in Miniature Swine,'' Exp. Neurol., **126**, pp. 291–299.

[29] Grady, M. S., McLaughlin, M. R., Christman, C. W., Valadka, A. B., Fligner, C. L., and Povlishock, J. T., 1993, ''The Use of Antibodies Targeted Against the Neurofilament Subunits for the Detection of Diffuse Axonal Injury in Humans,'' J. Neuropathol. Exp. Neurol., **52**, pp. 143–152.

[30] Gultekin, S. H., and Smith, T. W., 1994, ''Diffuse Axonal Injury in Craniocerebral Trauma,'' Arch. Pathology Laboratory Medicine, **118**, pp. 168–171.

[31] Sloan, K., Stevenson, J., and Bigbee, J., 1991, ''Qualitative and Quantitative Comparison of the Distribution of Phosphorylated and Non-Phosphorlyated Neurofilament Epitopes Within Central and Peripheral Axons of Adult Hamster (Mesocricetus Auratus),'' Cell Tissue Res., **263**, pp. 265–270.

[32] Rosenfield, J., Dorman, M. E., Griffin, J. W., Sternberger, L. A., Sternberger, N. H., and Price, D. L., 1987, ''Distribution of Neurofilament Antigens After Axonal Injury,'' J. Neuropathol. Exp. Neurol., **46**, pp. 269–282.

[33] Tomei, G., Spagnoli, D., Ducati, A., Landi, A., Villani, R., Fumagalli, G., Sala, C., and Gennarelli, T. A., 1990, ''Morphology and Neurophysiology of Focal Axonal Injury Experimentally Induced in the Guinea Pig Optic Nerve,'' Acta Neuropathologica, **80**, pp. 506–513.

[34] Sokol, S., 1976, ''Visually Evoked Potentials: Theory, Techniques, and Clinical Applications,'' Surv. Ophthalmol., **21**, pp. 18–44.
[35] Mahapatra, A. K., and Bhatia, R., 1989, ''Predictive Value of Visual Evoked Potentials in Unilateral Optic Nerve Injury,'' Surg. Neurol., **31**, pp. 339–342.
[36] Harding, G., 1984, ''A Flash of Light: A Personal Review of 21 Years of Study of the Electrical Activity of the Visual Pathway Beyond the Retina,'' Ophthalmic Physiol. Opt., **4**, pp. 293–304.
[37] Gennarelli, T. A., Thibault, L. E., Tipperman, R., Tomei, G., Sergot, R., Brown, M., Maxwell, W. L., Graham, D. I., Adams, J. H., Irvine, A., Gennarelli, L. M., Duhaime, A. C., Boock, R., and Greenberg, J., 1989, ''Axonal Injury in the Optic Nerve: A Model Simulating Diffuse Injury in the Brain,'' J. Neurosurg., **71**, pp. 244–253.
[38] Creel, D. J., 1972, ''Retinogeniculostriate Projections in Guinea Pigs: Albino and Pigmented Strains Compared,'' Exp. Neurol., **36**, pp. 411–425.
[39] Creel, D. J., Dustman, R. E., and Beck, E. C., 1973, ''Visually Evoked Responses in the Rat, Guinea Pig, Cat, Monkey, and Man,'' Exp. Neurol., **40**, pp. 351–366.
[40] Ducati, A., Fava, E., and Motti, E. D. F., 1988, ''Neuronal Generators of the Visual Evoked Potentials: Intracerebral Recording in Awake Humans,'' Electroencephalogr. Clin. Neurophysiol., **71**, pp. 89–99.
[41] Apaydin, C., Oguz, Y., Agar, A., Yargicoglu, P., Demir, N., and Aksu, G., 1993, ''Visual Evoked Potentials and Optic Nerve Histopathology in Normal and Diabetic Rates and Effect of Ginkgo Biloba Extract,'' Acta Ophthalmol., **71**, pp. 623–628.
[42] Suzuki, M., Sitizyo, K., Takeuchi, T., and Saito, T., 1991, ''Visual Evoked Potential From Scalp in Guinea Pigs,'' J. Veterinary Medicine Science, **53**, pp. 301–305.
[43] Suzuki, M., Sitizyo, K., Takeuchi, T., and Saito, T., 1991, ''Changes in the Visual Evoked Potentials With Different Photic Conditions in Guinea Pigs,'' J. Veterinary Medicine Science, **53**, pp. 911–915.
[44] Takeuchi, T., Suzuki, M., Sitizyo, K., Isobe, R., Saito, T., Umemura, T., and Shimada, A., 1992, ''Visual Evoked Potentials in Guinea Pigs With Brain Lesion,'' J. Veterinary Medicine Science, **54**, pp. 813–820.
[45] Altman, D., 1991, *Practical Statistics for Medical Research*, Chapman & Hall, New York.
[46] Swensen, S., Silverstein, M., Ilstrup, D., Schleck, C., and Edell, E., 1997, ''The Probability of Malignancy in Solitary Pulmonary Nodules: Application to Small Radiologically Indeterminate Nodules,'' Arch. Internal Medicine, **157**, pp. 849–855.
[47] Garber, B., Hebert, P., Wells, G., and Yelle, J., 1996, ''Validation of Trauma and Injury Severity Score in Blunt Trauma Patients by Using a Canadian Trauma Registry,'' J. Trauma, **40**, pp. 733–737.
[48] Shalev, A., Freedman, S., Peri, T., Brandes, D., and Sahar, T., 1997, ''Predicting PTSD in Trauma Survivors: Prospective Evaluation of Self-Report and Clinician-Administered Instruments,'' Br. J. Psychiatry, **170**, pp. 558–564.
[49] Ukimura, O., Troncoso, P., Ramirez, E., and Babaian, R., 1998, ''Prostate Cancer Staging: Correlation Between Ultrasound Determined Tumor Contact Length and Pathologically Confirmed Extraprostatic Extension,'' J. Urol., **159**, pp. 1251–1259.
[50] Varela, A., Bosco Lopez Saez, J., and Quintela Senra, D., 1997, ''Serum Ceruloplasmin as a Diagnostic Marker of Cancer,'' Cancer Lett., **121**, pp. 139–145.
[51] Bytzer, P., Moller Hansen, J., Schaffalitzky de Muckadell, B., and Malchow-Moller, A., 1997, ''Predicting Endoscopic Diagnosis in the Dyspeptic Patient: The Value of Predictive Score Models,'' Scand. J. Gastroenterol., **32**, pp. 118–125.
[52] Allaouchiche, B., Jaumain, H., Dumontet, C., and Motin, J., 1996, ''Early Diagnosis of Ventilator-Associated Pneumonia: Is It Possible to Define a Cut-off Value of Infected Cells in BAL Fluid?'' Chest, **110**, pp. 1558–1565.
[53] Peipert, J., Boardman, L., Hogan, J., Sung, J., and Mayer, K., 1996, ''Laboratory Evaluation of Acute Upper Genital Tract Infection,'' Obstet. Gynecol. (N.Y.), **87**, pp. 730–736.
[54] Pastor, A., Menendez, R., Cremades, M., Pastor, V., Llopis, R., and Aznar, J., 1997, ''Diagnostic Value of SCC, CEA, and CYFRA 21.1 in Lung Cancer: A Bayesian Analysis,'' Eur. Respir. J., **10**, pp. 603–609.
[55] Duke, T., Butt, W., and South, M., 1997, ''Predictors of Mortality and Multiple Organ Failure in Children With Sepsis,'' Intensive Care Med., **23**, pp. 684–692.
[56] Fijten, G., Starmans, R., Muris, J., Schouten, H., Blijham, G., and Knottnerus, J., 1995, ''Predictive Value of Signs and Symptoms for Colorectal Cancer in Patients With Rectal Bleeding in General Practice,'' Fam. Pract., **12**, pp. 279–286.
[57] Einstein, A., Bodian, C., and Gil, J., 1997, ''The Relationships Among Performance Measures in the Selection of Diagnostic Tests,'' Arch. Pathol. Lab Med., **121**, pp. 110–117.
[58] Diamond, G., 1992, ''Clinical Epistemology of Sensitivity and Specificity,'' J. Clin. Epidemiol., **45**, pp. 9–13.
[59] Hajian-Tilaki, K., Hanley, J., Joseph, L., and Collet, J., 1997, ''A Comparison of Parametric and Nonparametric Approaches to ROC Analysis of Quantitative Diagnostic Tests,'' Med. Decis Making, **17**, pp. 94–102.
[60] MacKillop, W., and Quirt, C., 1997, ''Measuring the Accuracy of Prosnostic Judgments in Oncology,'' J. Clin. Epidemiol., **50**, pp. 21–29.
[61] Heshner, D., and Johnson, L. W., 1981, *Applied Discrete Choice Modeling*, Croom Helm, London.
[62] Steinberg, D., and Colla, P., 1991, *LOGIT: A Supplementary Module for SYSTAT*, SYSTAT, Inc., Chicago.
[63] Sima, A. A. F., Zhang, W. X., Cherian, P. V., and Chakrabarti, S., 1992, ''Impaired Visual Evoked Potential and Primary Axonopathy of the Optic Nerve in the Diabetic BB/W-Rat,'' Diabetologia, **35**, pp. 602–607.
[64] Myers, B., Van Ee, C., Camacho, D., Woolley, C., and Best, T., 1995, ''On the Structural and Material Properties of Mammalian Skeletal Muscle and Its Relevance to Human Cervical Impact Dynamics,'' in: *Proc. 39th Stapp Car Crash Conference*, SAE, Coronado, CA.
[65] Myers, B. S., Best, T. M., Wooley, C. T., and Camacho, D. L., 1994, ''Measurement of Large Strain in Skeletal Muscle,'' in: *Proc. 22nd Annual International Workshop on Human Subjects for Biomechanical Research*, Fort Lauderdale, FL.
[66] Carrington Reid, M., Lane, D., and Feinstein, A., 1998, ''Academic Calculations Versus Clinical Judgments: Practicing Physicians' Use of Quantitative Measurements of Test Accuracy,'' Am. J. Med., **104**, pp. 374–380.
[67] Brenneman, F., Boulanger, B., McLellan, B., and Redelmeier, D., 1998, ''Measuring Injury Severity: Time for a Change?'' J. Trauma, **44**, pp. 580–582.
[68] Fine, B., and Yanoff, M., 1979, *Ocular Histology*, 2nd ed., Harper & Row, New York.
[69] McIntosh, T. K., Smith, D. H., Meaney, D. F., Kotapka, M. J., and Graham, D. I., 1996, ''Neuropathological Sequelae of Traumatic Brain Injury: Relationship to Neurochemical and Biomechanical Mechanisms,'' Lab. Invest., **74**, pp. 315–342.
[70] Ommaya, A. K., Yarnell, P., Hirsch, A. E., and Harris, E. H., 1967, ''Scaling of Experimental Data on Cerebral Concussion in Sub-Human Primates to Concussion Threshold for Man,'' in: *Proc. 13th Stapp Car Crash Conference*, SAE, Anaheim, CA.
[71] Bain, A. C., Billiar, K. L., Shreiber, D. I., McIntosh, T. K., and Meaney, D. F., 1996, ''In Vivo Mechanical Thresholds for Traumatic Axonal Damage,'' in: AGARD Specialists Meeting, Mescalero, NM.